

DISTRIBUTED AND ADAPTIVE FAST MULTIPOLE METHOD IN THREE DIMENSIONS

JONATHAN BULL AND STEFAN ENGBLOM

ABSTRACT. We develop a general distributed implementation of an adaptive fast multipole method in three space dimensions. We rely on a balanced type of adaptive space discretisation which supports a highly transparent and fully distributed implementation. A complexity analysis indicates favorable scaling properties and numerical experiments on up to 512 cores and 1 billion source points verify them. The parameters controlling the algorithm are subject to in-depth experiments and the performance response to the input parameters implies that the overall implementation is well-suited to automated tuning.

1. INTRODUCTION

The N -body problem is one of the most fundamental problems in computational physics and it has attracted considerable interest from researchers in numerical algorithms. For the computation of all pairwise particle interactions, the computational complexity of the immediate double for-loop algorithm scales as $\mathcal{O}(N^2)$. For large enough N and high enough tolerance requirements, it is known that the Fast Multipole Method (FMM) [11] stands out as an optimal algorithm of $\mathcal{O}(N)$ complexity, and which also achieves this optimal performance in practice. There is a steadily growing body of research into the use of FMM for the solution of integral equations and PDEs [1, 6, 9, 14, 30].

FMMs offer a linear complexity in N and enjoy sharp *a priori* error estimates, but due to their tree-based nature they are also notoriously hard to implement, particularly so in three spatial dimensions [4]. With modern multicore and distributed computer systems, there is an increased interest in designing effective parallelization strategies [2, 7, 12, 13, 15, 16, 26, 27]. Balancing efficiency with implementation transparency is here an important aspect [19, 23].

When source points are non-uniformly distributed it becomes necessary to adapt the FMM tree according to the local point density such that the computational effort is balanced across the tree. Mesh adaptivity, while solved in theory already in the early ages of the FMM [25], becomes a major issue when confronted with parallelism due to the associated complicated memory access patterns. Early attempts to mitigate this through post-balancing algorithms [21] are less attractive for complexity reasons, and when data-parallel accelerators made their debut a decade ago, it was in fact suggested that non-adaptive FMMs offer a better performance [12].

Date: February 13, 2020.

2010 Mathematics Subject Classification. Primary: 65Y05, 68W10; Secondary: 65Y10, 65Y20, 68W15.

Key words and phrases. Adaptive fast multipole method; Distributed parallelisation; Message Passing Interface (MPI); Multipole acceptance criterion; Balanced tree.

Corresponding author: S. Engblom, telephone +46-18-471 27 54, fax +46-18-51 19 25.

In this paper we describe the development of a variant of the adaptive FMM, the balanced tree FMM [8, 10, 13], in three dimensions and using distributed parallelisation on very large modern computer systems. Rather than adapting the number of levels locally as in the classic adaptive FMM, our balanced tree FMM maintains a fixed number of levels and splits boxes at median planes such that the number of points in each subtree is balanced at every level. Otherwise known as orthogonal recursive bisection (ORB) [20, 24, 28], it is guaranteed to produce a balanced tree [28].

The implementation of the balanced tree FMM with distributed parallelism is relatively straightforward and is shown to scale well up to 512 processes at a respectable absolute efficiency. Furthermore, it exposes various parameters to the user enabling the performance to be readily optimised for a particular simulation. We show that the performance response is convex in the parameter space making the balanced tree FMM particularly well-suited to automatic tuning in an online computing context.

Since the FMM has been judged to be one of the top 10 most important algorithms of the 20th century [5], it is our hope that insights obtained here is of general value. Our implementation of the parallel balanced tree FMM is therefore freely available as `daFMM3D` (distributed adaptive FMM in 3D) C/C++/Matlab code at www.stenglib.org.

The structure of the paper is as follows: in §2 we describe the balanced tree FMM in three dimensions including the multipole acceptance criterion, adaptive box splitting and computational complexity estimates. The corresponding distributed algorithm is also presented with a description of parallel data structures and communication complexity. In §3 convergence test results, parameter response test results and and strong scaling results on up to 512 processes are reported. The algorithm's adaptive response is also tested in the more challenging case of a spiral galaxy of 1 billion sources with a multiscale structure.

2. 3D BALANCED TREE FMM IN A DISTRIBUTED ENVIRONMENT

Fast multipole methods evaluate pairwise interactions of the type

$$(2.1) \quad \Phi(x_i) = \sum_{j=1, j \neq i}^N G(x_i, x_j), \quad x_i \in \mathbf{R}^D, \quad i = 1 \dots N,$$

where $D = 3$ in this paper, and where $\{x_j\}$ are a set of N *sources* (points) in a force field governed by the kernel G . The FMM is a tree-based algorithm that produces a continuous representation of the field such that it can be evaluated to within the tolerance anywhere inside a bounding box enclosing the sources.

2.1. Adaptivity and complexity. The sources are initially placed in a single bounding box at level $l = 0$ of the tree. Splitting operations produce child boxes on levels $l > 0$, with the number of points per box becoming successively smaller with each level. Each box is given an outgoing *multipole* expansion and an incoming *local* expansion. The multipole expansion is valid far away from the box and is the expansion of all the points in the box about the box centre. In 3D it is the spherical harmonics expansion [3]. The local expansion is valid within the box and is the expansion of far-away sources about the box centre. Both the multipole and local expansions are of order Q which determines the overall precision.

2.1.1. *The θ -criterion.* We consider the *balanced tree* version of FMM as described in [8]. As with the original FMM, boxes on the same level are either unconnected or strongly/weakly connected depending on the separation of their centres. A pair of boxes with radii r_1 and r_2 and separation d are deemed to be weakly connected if the *theta criterion* is satisfied:

$$(2.2) \quad R + \theta r \leq \theta d,$$

where $R = \max(r_1, r_2)$, $r = \min(r_1, r_2)$ and $\theta \in (0, 1)$ is a parameter. If the criterion is not satisfied then the boxes are strongly connected. The choice of θ affects the *connectivity pattern*, i.e., the stencil of strongly and weakly connected boxes, and thus the relative amount of work spent on different parts of the algorithm. In practice it has been found that $\theta = 0.5$ leads to a well balanced algorithm in 2D for various source densities [10], however, we will reevaluate the optimal value for different point distributions in 3D in this paper. Boxes inherit connections from their parents: the children of strongly connected parents are allowed to be strongly or weakly connected to each other, as judged by (2.2), whereas the children of weakly connected parents are not connected.

2.1.2. *Adaptivity.* A balanced tree, or a *pyramid*, is one in which all boxes at level l are either subdivided further into level $l + 1$, or form the *leafs* of the tree, i.e., the boxes at the finest level. Traditional level-adaptive FMMs [4, 25] work by adjusting the number of levels locally, resulting in equal-sized boxes and an unbalanced tree. The balanced tree FMM [8], by contrast, keeps the number of levels fixed but each box is adaptively split along median planes such that the child boxes contain about an equal number of points, implying a pyramid tree. This results in different-sized boxes and a variable connectivity pattern, but crucially avoids the cross-level communication required by level-adaptive FMM.

For additional control over the tree we introduce an adaptivity parameter, $\eta \in [0, 1]$. $\eta = 0$ enforces splitting at geometric mean planes resulting in a non-adaptive or fixed tree where all children are the same size and there are a uniform number of connections between boxes, thus balancing the cost of the Multipole-to-Local (M2L) shift. $\eta = 1$ instead splits boxes at median planes such that all children contain about an equal number of sources, thus balancing the cost of the Particle-to-Particle (P2P) shift. One may set η in between 0 and 1 to split at a weighted average of the geometric mean and the source point median. This may be useful for tuning the performance in individual simulations. A similar approach splitting at the n th element has been used to balance loads between arbitrary numbers of parallel processes [28].

2.1.3. *Computational Complexity.* The cost of the FMM is dominated by the M2L and P2P shifts. We evaluate the complexity of these two operations in the 3D balanced tree FMM with $\eta = 1$ and θ arbitrary. It is assumed that the mesh is asymptotically regular so that $R \approx r$ in (2.2) and that there are M boxes at the finest level.

Each box is weakly connected to boxes within a spherical shell whose inner surface is defined by (2.2), $d = (1 + \theta)/\theta \times r$. The outer surface is defined by strong connections at the parents' level, $d_{\text{parent}} = (1 + \theta)/\theta \times r_{\text{parent}} = 2d$. This shell contains approximately $d^3 M$ boxes. By approximating the separation $r \sim M^{-1/3}$, we arrive at an estimate of $\mathcal{O}(\theta^{-3})$ weak connections per box. M2L in its basic form scales as $\mathcal{O}(Q^4)$ [3]. We use the rotational translation form which rotates the

z -axis of the spherical harmonic expansion to the vector from one box to another. This form requires $\mathcal{O}(Q^3)$ operations per pair so the complexity of the M2L shift for all M boxes is $\mathcal{O}(Q^3\theta^{-3}M)$. The exponential plane wave expansion form scales as $\mathcal{O}(Q^2)$ [3], but it is not practical to use in the balanced tree FMM because the geometric relationships are not fixed *a priori*.

Each box is strongly connected to $\frac{4}{3}\pi d^3 M$ boxes in a sphere, each containing N/M sources. The P2P evaluation requires $\mathcal{O}(N^2 M^{-2})$ operations per pair of boxes so the total cost of P2P is $\mathcal{O}(N^2\theta^{-3}M^{-1})$. If we always set the number of levels such that N/M is constant this becomes $\mathcal{O}(\theta^{-3}N)$. To balance the M2L and P2P operations we require that the number of source points per leaf is related to the order of the multipole expansion: $(N/M)^2 \propto Q^3$.

In practice, the assumption of asymptotic regularity may not be satisfied, particularly for low numbers of levels and highly inhomogeneous source distributions, leading to different scaling than the above estimates. However, with the free parameters L (which determines the ratio N/M), θ and η it is possible to tune the balanced tree FMM for a specific source distribution.

2.2. Distributed adaptive FMM. This section describes the parallelisation of the balanced tree FMM for N points with $L + 1$ levels $l \in \{0, 1, 2, \dots, L\}$ in a distributed memory framework on P processes. The balanced tree FMM requires the construction of a connectivity matrix since geometric relationships between boxes are not fixed *a priori*. In parallel, this connectivity matrix has to be partially shared between processes.

2.2.1. Data Structures. In the FMM octree T we refer to the box on level 0, denoted $T^{(0)}$, as the global root. It is split into P boxes on level 1, the local roots $T_p^{(1)}$. Each process p then constructs its own L -level local octree T_p with local root $T_p^{(1)}$ and leaf level $T_p^{(L)}$. The j th box on level l is denoted $T_{p,j}^l$.

Since the connectivity pattern is not fixed in the balanced tree FMM, supporting data structures are required. On levels $l = 1 : L$ each process p constructs a local compressed column storage (CCS) format sparse connectivity matrix $C_p^{(l)}$ encoding same-level connections within T_p , as well as $P - 1$ (possibly empty) halo matrices $H_{pq}^{(l)}$ encoding same-level connections to $T_q, q \neq p$. Together, all $C^{(l)}$ and $H^{(l)}$ matrices form a global connectivity matrix on level l . The halos are symmetric ($H_{qp}^{(l)} = (H_{pq}^{(l)})^T$) so only the lower-triangular part of the global matrix needs to be constructed, however to reduce communication each process constructs all $P - 1$ halos itself. Figure 2.1 illustrates a distributed FMM octree.

Each halo $H_{pq}^{(l)}$ contains a sparse matrix in index-format that stores all the pairs of strongly and weakly connected boxes owned by processes p and q . The index-sparse format utilises two lists, `ibox` and `jbox`, containing the indices of boxes in p and q , respectively. In the FMM, boxes can only interact if their parents are strongly connected, hence $H_{pq}^{(l)}.ibox$ is 64 times larger than $H_{pq}^{(l-1)}.ibox$; likewise for $H_{pq}^{(l)}.jbox$. The index-sparse format implies that a box appears k times if it has k connections. The format has been chosen since it compresses better than the CCS format when only a small subset of the boxes are connected. This condition is true for large l where only a very thin layer of boxes on the subdomain surface are connected across the process boundary.

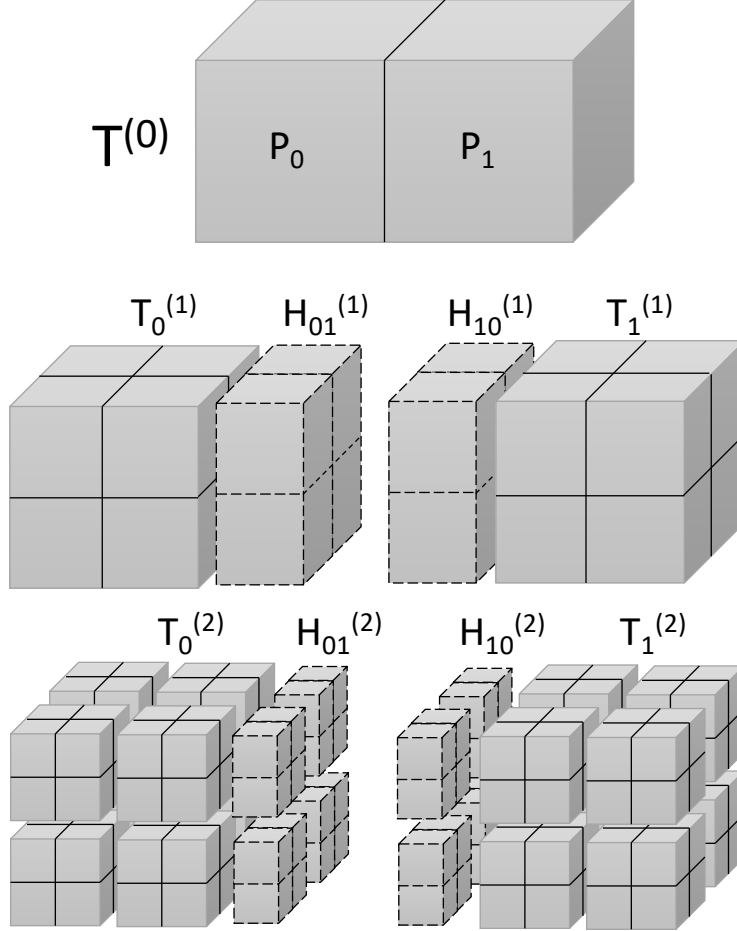


FIGURE 2.1. Schematic of a 2-process distributed tree with 3 levels. Halos are shown as boxes with dashed outlines. Subscripts denote parallel processes and superscripts denote tree level.

2.2.2. *Distributed algorithm.* Algorithm 1 describes the whole distributed balanced tree FMM for P processes and an $L + 1$ level octree. Construction of the balanced tree, connectivity matrix and halo matrix (Tree subroutine) are described in Algorithm 2 in the Appendix. The downward pass of the balanced tree FMM (M2L, L2L subroutines) is described in Algorithm 3. The direct evaluation (P2P, L2P subroutines) is described in Algorithm 4. It is assumed that data partitioning onto P processes is done in a separate preprocessing step, mimicking the intended use as a plugin solver for other scientific applications.

2.2.3. *Computational Complexity.* Besides the M2L and P2P shifts, which dominate the cost of FMM, there is a cost associated with halo construction in the distributed balanced tree FMM. Halo construction, detailed in Algorithm 2, has computational complexity of $\mathcal{O}(N)$.

Algorithm 1 Distributed balanced tree FMM.

```

1: for all  $p \in P$  do
   Alloc:
2:   allocate arrays for tree  $T_p$  on all levels and for points on level  $L$ 
   Tree (construction of  $T_p, C_p, H_p$ ):
3:   Algorithm 2
   P2M:
4:   Compute multipole expansions on level  $L$  from point data
   M2M (Upward pass of tree  $T_p$ ):
5:   for  $l = L : 2$  do
6:     compute multipole expansions in  $T_p^{(l-1)}$  from children in  $T_p^{(l)}$ 
7:   end for
   M2L, L2L (Downward pass of tree  $T_p$ ):
8:   Algorithm 3
   L2P, P2P (Direct valuation of potentials on leaf level  $L$ ):
9:   Algorithm 4
10:  end for

```

2.2.4. *Communication Complexity.* Communication is dominated by the P2P interaction amongst N sources. Let the domain with $\mathcal{O}(1)$ volume be divided equally into P subdomains and assume that P is sufficiently large that relatively few processes lie on the domain boundary. The communication complexity is proportional to the number of sources lying close to each subdomain's boundaries with other subdomains. Each subdomain has a surface area of $\mathcal{O}(P^{-2/3})$ and there are $\mathcal{O}(N^{2/3})$ sources per unit area. This leads to the estimate of $\mathcal{O}((N/P)^{2/3})$ for the communication complexity as calculated in [29]. There is also a contribution of $\mathcal{O}((M/P)^{2/3})$ for the M2L shift between M boxes but since we let N/M be constant this is included in the above estimate. Similarly the halo requires communication of the positions and dimensions of M boxes which can be included in the above estimate.

2.2.5. *Summary.* The distributed balanced tree FMM is designed to allow easy tuning/optimisation for a particular distribution of sources by exposing the parameters of relevance to the algorithm. It is relatively straightforward to implement and memory access is simpler than in the classic level-adaptive FMM. The additional cost of halo construction and communication is negligible.

3. COMPUTATIONAL EXAMPLES

The distributed balanced tree FMM has been implemented in a C/C++/MPI code named `daFMM3D` available at www.stenglib.org. In serial it can be run via a Matlab interface. The code solves N -body problems subject to forces that follow an inverse-square law such as gravitation, although other kernels can be implemented analogously.

3.1. **Convergence.** Engblom (2011) [8] derived that the relative error of the balanced tree FMM solution ϕ for N positive potentials under the theta criterion is bounded by a factor $C\theta^{p+1}/(1-\theta)^2$, where C is a constant. We verify that this bound is satisfied by the present implementation for a set of $N = 1000$ random

points at N different random evaluation points in 3D. A reference solution ϕ_0 is computed by direct evaluation and the FMM solutions ϕ_k are computed with tolerances of 10^{-k} for $k = 1, 2, \dots, 15$. Figure 3.1 shows the relative error $e_k = |(\phi_0 - \phi_k)/\phi_0|$ together with the theoretical bound.

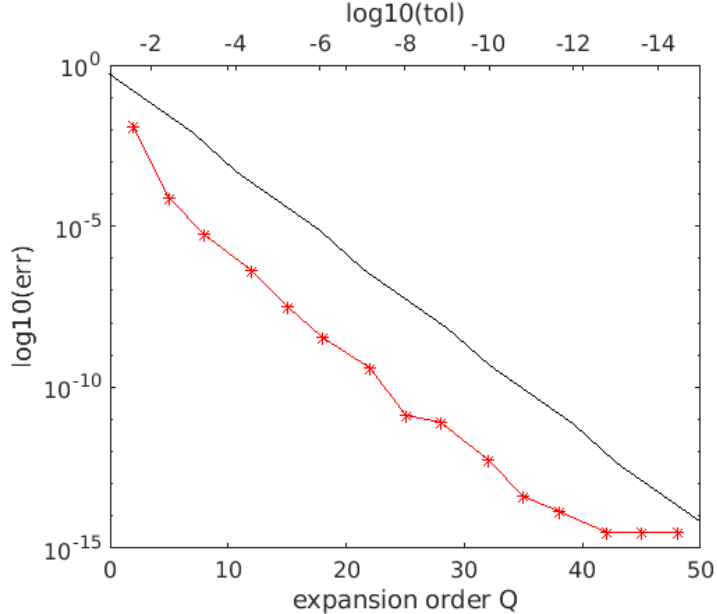


FIGURE 3.1. Convergence of relative error in FMM solution. The upper x -axis shows the tolerance and the lower x -axis the polynomial order of the expansions.

3.2. Parameter response. The sensitivity of the balanced tree FMM to the free parameters θ , η and L was investigated for four different distributions of 100,000 points on a single process. In this study the error tolerance was fixed to $\text{TOL} = 10^{-6}$. The four distributions were (a) randomly distributed points in the unit cube, (b) spherical Gaussian distribution, (c) spherical shell and (d) a helix. These distributions were chosen with the intent to ‘stress-test’ the adaptive response of the algorithm. The three independent parameters were varied in the ranges $0 \leq \theta \leq 0.8$, $1 \leq L \leq 4$, $0 \leq \eta \leq 1$. While varying one parameter the remaining two were set to default values ($\theta = 0.5$, $\eta = 0.5$ and $L = 3$) so although this is not a full sweep of parameter space, it gives a reasonably good understanding of the performance response.

The code was executed 4 times for each combination of parameters. Figures 3.2, 3.3 and 3.4 show the normalised mean time curves against θ , η and L respectively, with error bars denoting the minimum and maximum times. Times were normalised by the mean times at $\theta = 0.5$, $\eta = 0$ and $L = 1$. Table 3.1 lists the optimal parameter values identified from the graphs.

All cases are highly sensitive to θ . Run times for the random, shell and spiral cases are minimised in the range $0.4 < \theta < 0.6$, consistent with a previous result in 2D [8]. The Gaussian case has minimum run time at $0.3 < \theta < 0.5$ and it is

less sensitive to low θ than the other cases. Interestingly, none of the cases display a strong sensitivity to η . The Gaussian and shell cases have distinct minima (at $\eta \approx 0.5$ and $0.4 < \eta < 0.8$ respectively) but the times are only 5% less than at $\eta = 0$. The Gaussian case exhibits more variation in run times at large values of η than the other 3 cases. The optimal number of levels is 3 for the random, spiral and shell cases, corresponding to a maximum of 195 points per leaf box. Four levels is optimal for the Gaussian, about 24 points per leaf box.

The optimal values are a compromise between the M2L and P2P subroutines. M2L time increases with L and θ , whereas P2P time decreases with L and θ . Furthermore, the optimal values of L and θ are co-dependent: more levels increases the M2L time which biases the optimal θ towards lower values (reduced M2L time) and vice versa.

These results demonstrate that for a given distribution, it is generally not possible to determine the optimal parameters *a priori*. However, the clear convex response of total time to individually varying L and θ motivates the use of auto-tuning optimisation techniques where the parameters are adjusted in steps as the underlying simulation proceeds. L has the most drastic effect and could possibly be chosen *a priori* to result in a desired mean number of points per leaf (suggested range 50-200), leaving θ and η free to vary for fine tuning. The four tested distributions displayed little sensitivity to η , but this may be due to their limited size and complexity. In larger, more complex distributions we expect that η may play a larger role, as seen with the spiral galaxy in §3.4.

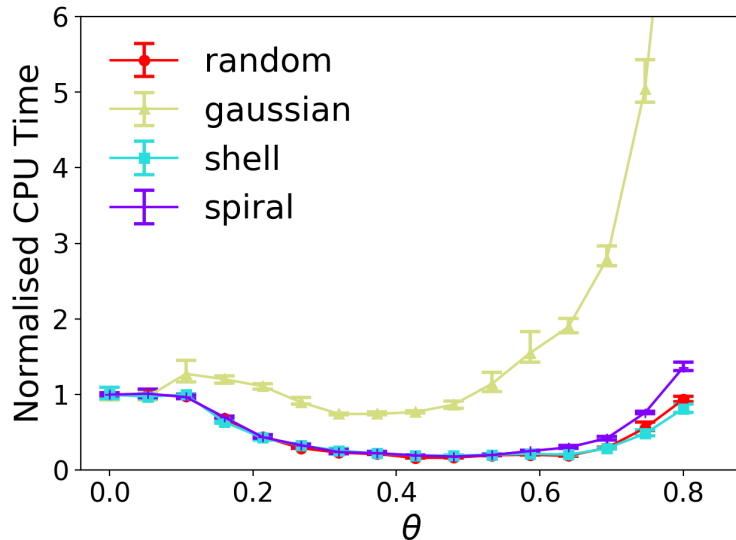


FIGURE 3.2. Sensitivity of total time to θ in the random, Gaussian, spiral and shell distributions of 100000 points.

3.3. Scaling. Strong and weak scaling is assessed for the `daFMM3D` code in non-adaptive mode ($\eta=0$, $\theta=0.5$) on a set of uniformly distributed points in the unit cube. They are partitioned into cubic numbers of processes ($1^3, 2^3, \dots$) so that the

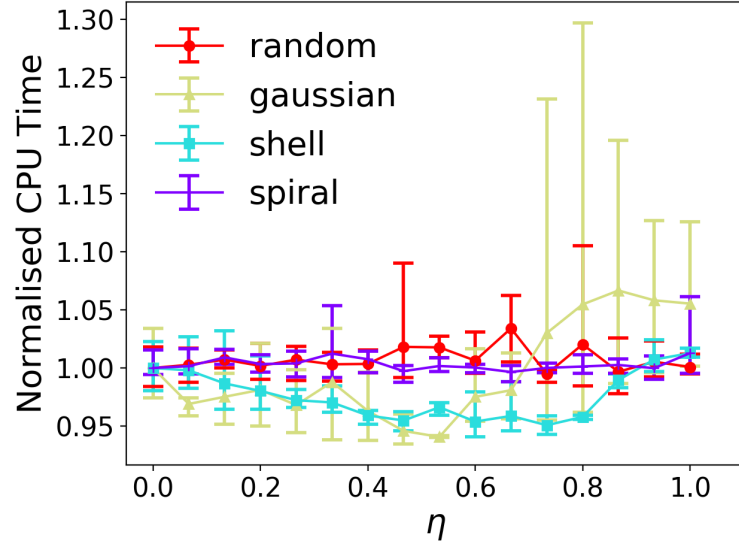


FIGURE 3.3. Sensitivity of total time to η in the random, Gaussian, spiral and shell distributions of 100000 points.

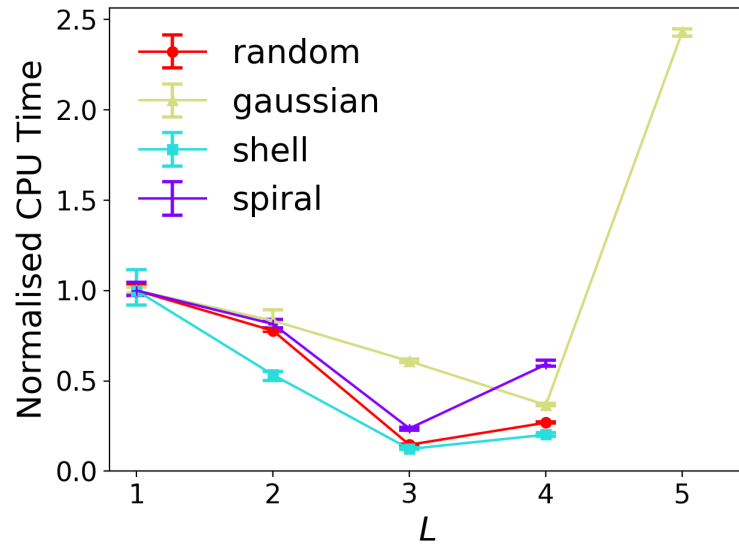


FIGURE 3.4. Sensitivity of total time to L in the random, Gaussian, spiral and shell distributions of 100000 points. Note 5 values for Gaussian and 4 for the other cases.

connectivity patterns are as close to identical as possible. To verify that balanced-tree adaptivity has no impact when the points are uniformly distributed the weak scaling tests were also run with $\eta = 1$. The total times and scaling efficiencies were

distribution	θ opt.	η opt.	L opt.
random	0.45	-	3
Gaussian	0.4	0.5	4
shell	0.5	0.4-0.8	3
helix	0.5	-	3

TABLE 3.1. Optimal parameter values in the random, Gaussian, spiral and shell distributions of 100000 points. A dash (-) means no optimum value could be identified (flat response curve).

near-identical to the non-adaptive algorithm. Every data point in the results is an ensemble average from a minimum of four separate runs.

Scaling tests were run on the Rackham cluster, part of the Uppmax computing service at Uppsala University. Rackham consists of 334 nodes each with two 10-core Xeon E5-2630 V4 processors running at 2.2 GHz (turbo 3.1 GHz) and 128 GB memory per node. All nodes are interconnected with a 2:1 oversubscribed FDR (56 GB/s) Infiniband fabric. When the requested number of processes fitted onto one node, that node's entire resources were reserved for that job, eliminating timing inconsistencies due to sharing the node with other jobs.

3.3.1. *Strong Scaling Results.* In the strong scaling tests $N=10M$ points were distributed over 1, 8, 64 and 512 processes with 7, 6, 5 and 4 levels in the global tree respectively. To ensure a fair comparison the number of levels was reduced as P increased so that the number of points per leaf box N/M was kept approximately constant ($N/M \approx 38$). Figure 3.5 shows the CPU time of the different subroutines as well as the total time. The strong scaling efficiency was 23.2% in these tests, and was mainly limited by the non-ideal scaling of Tree and P2P. Excluding these, the scaling efficiency of 56.2% was achieved. M2L was the dominant subroutine in these tests and it achieved an efficiency of 56.4%.

3.3.2. *Weak Scaling Results.* In the weak scaling tests 1M points were assigned to each process and up to 512 processes were used. In Figures 3.6, 3.7, and 3.8, (a) the maximum CPU times of each subroutine, (b) the normalised M2L and (c) normalised P2P times with 4, 5 and 6 levels, respectively, are reported. The total weak scaling efficiency of 62.9%, 46.2% and 49.4% is achieved with 4, 5 and 6 levels. The total time is strongly dependent on the number of levels: 5 levels (244 points/leaf) is about 4 times faster than 4 levels (1953 points/leaf) or 6 levels (31 points/leaf).

All subroutines except Tree achieve relatively good weak scaling with flat maximum times for $P > 27$. The increase in times from $P=1$ to $P=27$ is anticipated due to connectivity changes as discussed below. Poor scaling of the Tree subroutine is due to latency caused by waiting for non-blocking MPI receive commands to complete in process number order (Algorithm 2 line 22). Tree makes a negligible contribution to total time within the range of P tested but it will become significant at very large P ; this is easily mitigated by some additional software engineering. The M2L and P2P subroutines were implemented differently, with non-blocking receives being processed in the order in which they were completed to reduce latency (see Algorithm 3 lines 7-15 and Algorithm 4 lines 10-17).

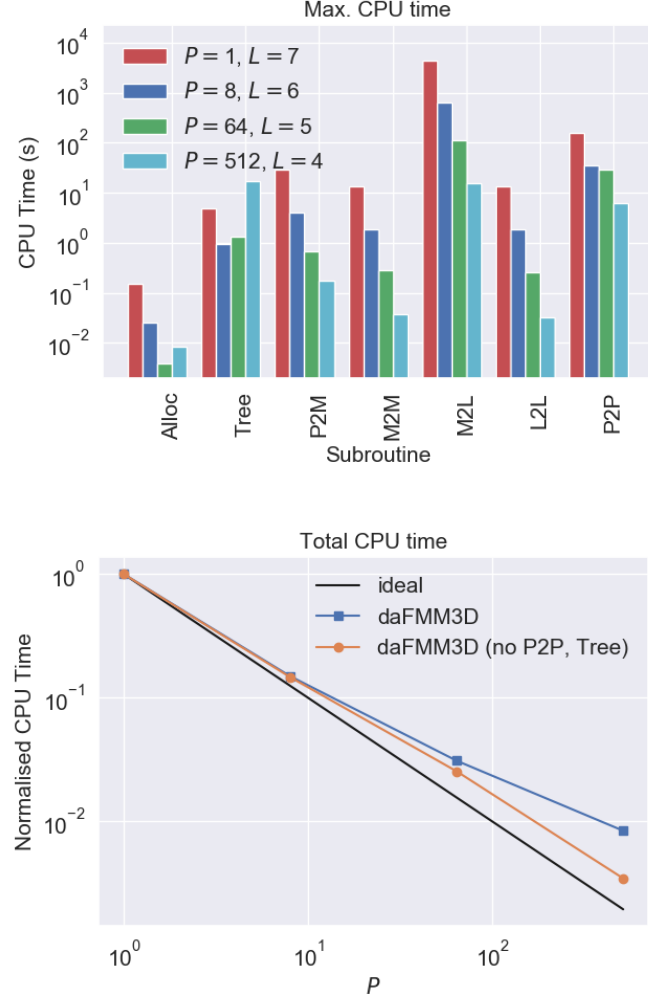


FIGURE 3.5. Strong scaling, 10M points, 1-512 processes, constant 38 points/leaf box. Top: time per subroutine, bottom: total time.

The number of levels influences the scaling of M2L and P2P differently: the best weak scaling of M2L is with 6 levels but the best scaling of P2P is with 4 levels. Conversely the shortest execution time for M2L is with 4 levels and for P2P with 6 levels. 5 levels offers the best balance of scaling efficiency and execution time for both subroutines and the lowest total execution time.

It is not possible to obtain perfect scaling of the FMM algorithm due to connectivity changing with the number of processes: as P increases a larger fraction of the subdomains do not have a boundary on the domain outer boundary so the average number of connections (especially far connections) to other processes increases. The largest growth in connectivity is from $P=1$ to $P=27$ and thereafter the increase in connectivity is marginal. Denoting the total number of

P	C_{near}	C_{far}
1	1	1
8	1.22	1.78
27	1.27	2.10
64	1.33	2.29

TABLE 3.2. Growth of total number of near and far connections with P relative to $P=1$ for 4-level weak scaling test setup.

levels	M2L (adjusted)	P2P (adjusted)	Total (adjusted)
4	21.7 (49.6)	64.2 (85.4)	62.9 (83.5)
5	41.7 (95.6)	56.5 (75.1)	46.2 (72.7)
6	56.1 (128.4)	9.3 (12.4)	49.4 (100.6)

TABLE 3.3. Weak scaling efficiencies of the M2L, P2P subroutines and total algorithm. Efficiencies obtained after adjusting for C_{near} and C_{far} are shown in parentheses.

near connections on the leaf level as N_{near} we define a near connectivity factor for P processes: $C_{near} = N_{near}/N_{near,P=1}$. Likewise the far connectivity factor is $C_{far} = N_{far}/N_{far,P=1}$ where N_{far} is the total number of far connections (all levels). Table 3.2 lists C_{near} and C_{far} for the 4-level weak scaling test up to $P=64$. To avoid burdensome calculations we assume that the 4-level, 64-process factors are good estimates of the factors that would be obtained with more levels and more processes.

In Figures 3.6-3.8 the orange lines show (b) the M2L times divided by C_{far} and (c) the P2P times divided by C_{near} for 4, 5 and 6 levels respectively. Table 3.3 lists the scaling efficiencies of M2L, P2P and the total algorithm without and with adjustment by C_{near} and C_{far} . The adjusted efficiencies of the total algorithm are 83.5%, 72.7% and 100.6% for 4, 5 and 6 levels respectively. The adjusted efficiencies of M2L for $L > 4$ are greater than 100%, suggesting that some of the extra connectivity burden at $P > 1$ may be hidden by efficiency gains obtained through good parallel execution (non-blocking calls and hiding latency with local computation). On the other hand, the adjusted P2P efficiencies are still low, showing that there is room for improvement in the parallelisation of this subroutine.

3.4. Load Balancing and Adaptivity. As a more complex test case we run a fairly realistic spiral galaxy of $N = 1B$ (10^9) points using 512 processes and a 5-level tree. The distribution was designed to give the model galaxy a multiscale structure representative of real spiral galaxies. The distribution forces the balanced tree FMM (with $\eta > 0$) to create a tree with boxes of varying aspect ratios and sizes in close proximity. We generated the final distribution from a set of 10,000 points in a rough toroidal shape with inner radius $R_{inner} \approx 6000$ and outer radius $R_{outer} \approx 18000$ parsecs. This initial set was generated by a Simulink model of two colliding galaxies [17, 22]. Figure 3.9 shows the initial set of 10,000 points and the boxes on level 2 generated with $\eta = 1$. Boxes are coloured according to which process they belong to ($P=8$ in this image). The axis of rotation of the galaxy is perpendicular to the page.

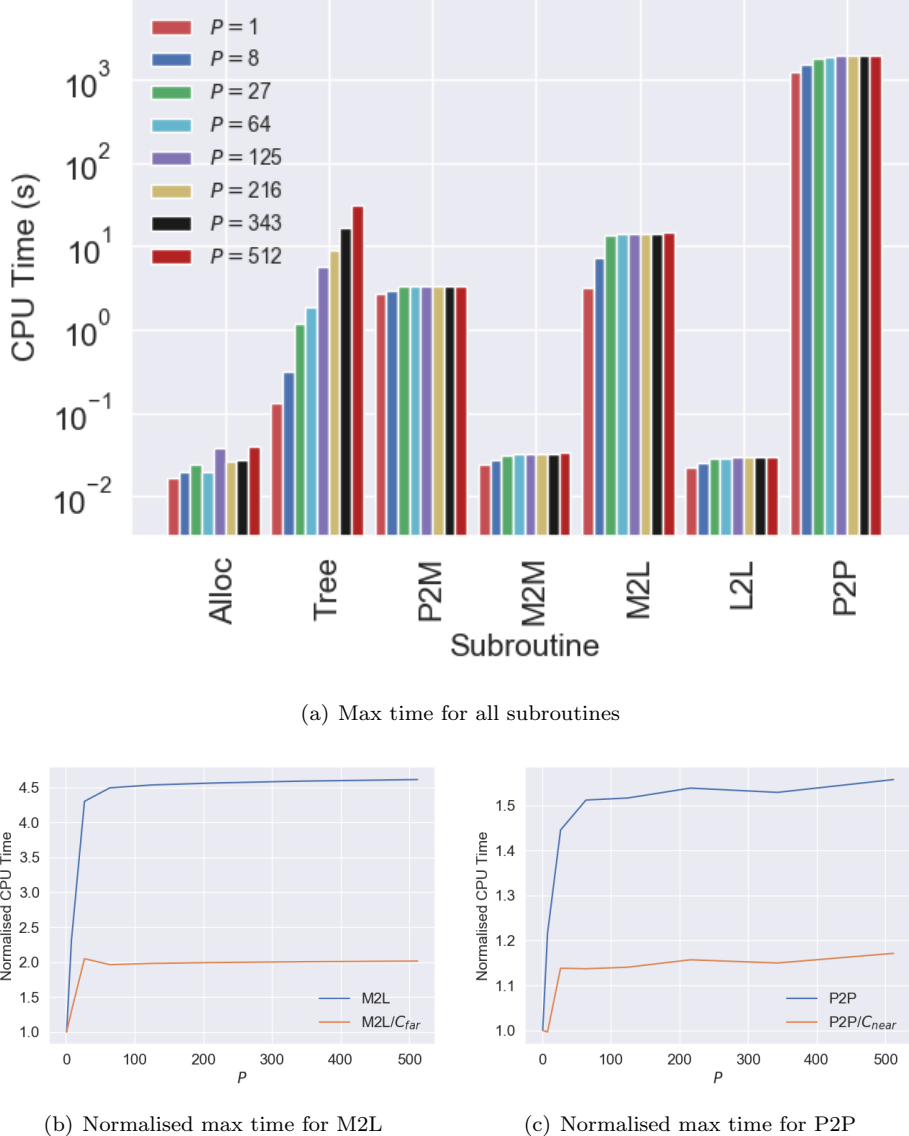


FIGURE 3.6. Weak scaling, 1M points/process, 1-512 processes, 4 levels.

The final distribution of 10^9 points was generated recursively from the initial set. For each of the 10,000 points a random distribution of 10 new points was created within an oblate spheroid centred on that point. The major axis of each spheroid was $R_0 = R_{\text{outer}}/20$ and the minor axis was $r_0 = R_0/10$ and parallel to the axis of rotation of the galaxy. For each of the 100,000 points in the new set (the original points having been deleted) the process was repeated with $R_1 = \frac{2}{3}R_0$ and $r_1 = R_1/10$, and so on until there were 10^9 points. The final set was partitioned into 512 subdomains arranged as an $8 \times 8 \times 8$ cube of subdomains containing 1,953,125

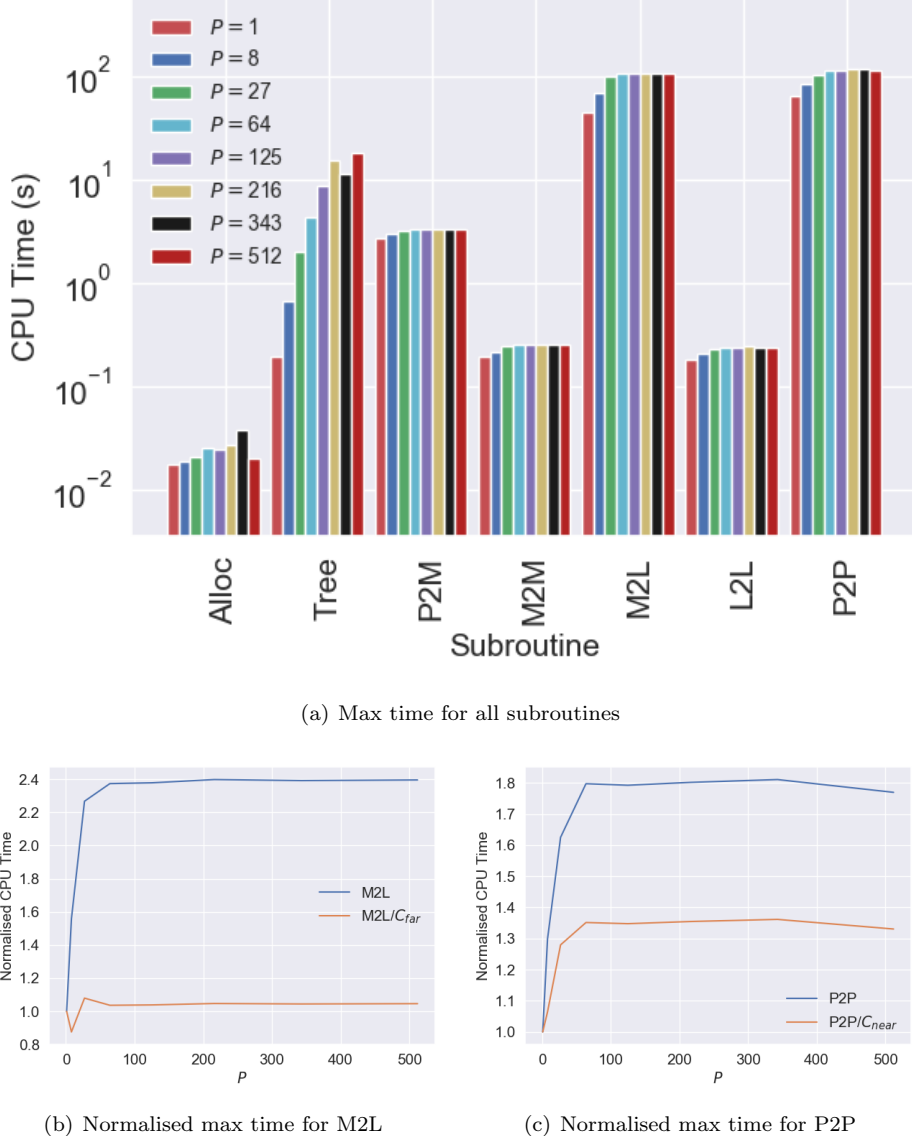


FIGURE 3.7. Weak scaling, 1M points/process, 1-512 processes, 5 levels.

points each. For simplicity our model only computes the force due to gravitational attraction, does not include a central black hole, and does not update the point velocities and positions.

The data was generated and the simulations were run on the Lomonosov-2 supercomputer at the Research Computing Center at Moscow State University, Russia. This computer was ranked 107(59) in the Top500 in November 2019 (June 2017) and has similar specifications to Rackham but 14 cores per node instead of 20.

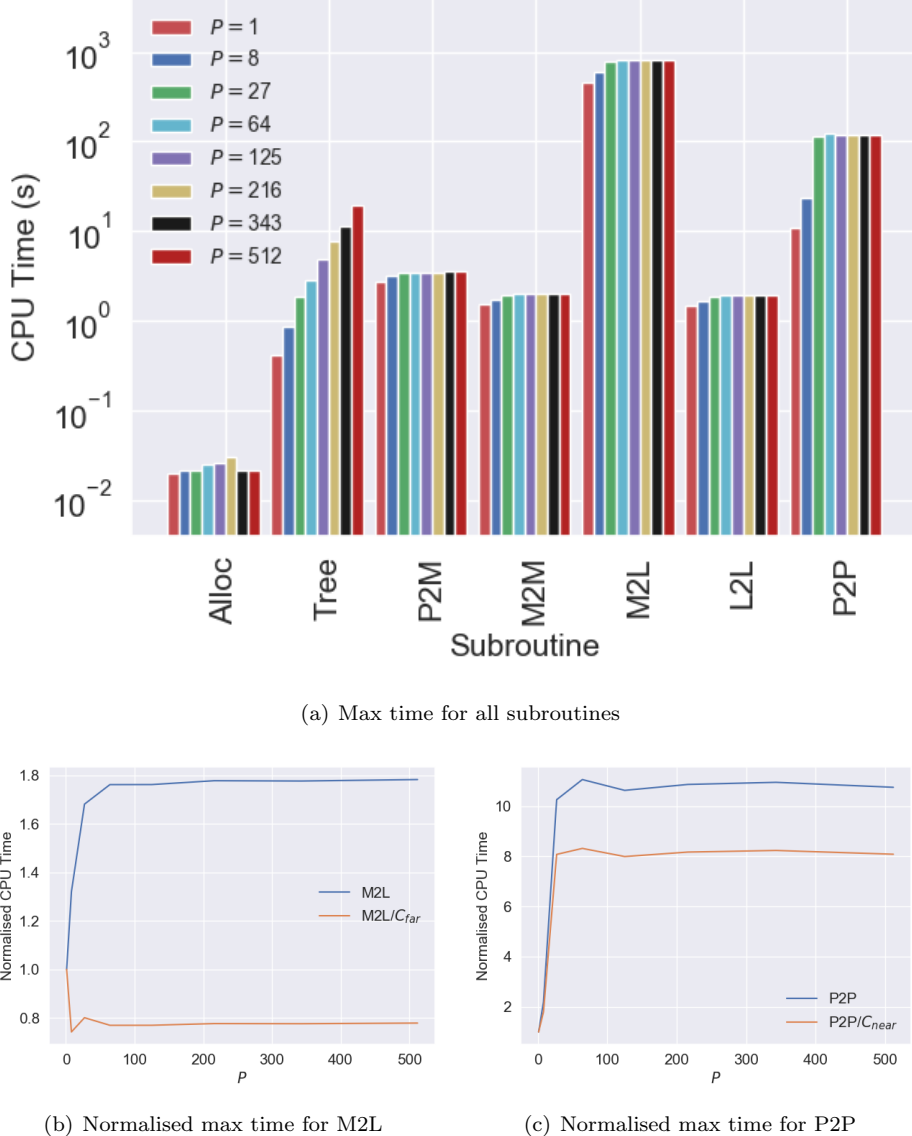


FIGURE 3.8. Weak scaling, 1M points/process, 1-512 processes, 6 levels

Figure 3.10 (a) shows individual subroutine times. Note that M2L times are shown separately for the serial M2L shift, labelled M2L (Algorithm 3 lines 17-19), and the parallel M2L shift, labelled M2Lh (lines 1-16 in Algorithm 3 lines 1-16). Figure 3.10 (b) shows the normalised total times (blue) for the galaxy evaluation with varying $\eta \in [0, 1]$. η mostly affects the performance of P2P in this test. The value that minimises total time is $\eta = 0.75$ which is 29% faster than $\eta = 1$ (fully adaptive FMM) and 57% faster than $\eta = 0$ (non-adaptive FMM). Figure 3.10 (b) also plots the variance in P2P time (orange), calculated as the difference between

maximum and minimum P2P times divided by the mean P2P time across all processes. This quantity is indicative of load balancing. The lowest variance in P2P time coincides with the minimum total time, suggesting that load balancing within P2P is important for efficient execution by reducing latency. Optimising over the adaptivity parameter η is an effective way to improve load balancing. Note, however, that even at $\eta = 0.75$ the maximum P2P time is 1.5 times longer than the minimum so there is room for further improvement.

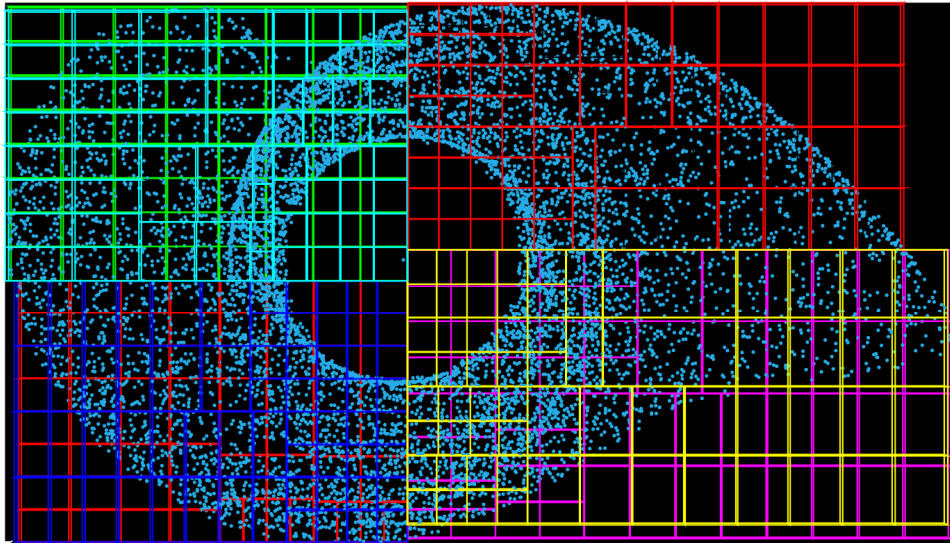


FIGURE 3.9. Initial 10,000-point spiral galaxy superimposed on the boxes at level 2 generated with $\eta = 1$. Colours indicate 8 different processes.

4. CONCLUSION

A 3D FMM algorithm with distributed parallelism employing balanced tree adaptivity has been described and tested. The balanced tree FMM is highly transparent with several key parameters exposed to user control. It is also relatively straightforward to implement in parallel and our code is freely available under a liberal licence at www.stenglib.org. We have demonstrated that the performance response of the balanced tree FMM in parameter space is well-defined or convex along individual parameters and thus is suited for automated optimisation.

Strong and weak scaling tests were performed on up to 512 processes using a modern multicore cluster. Strong scaling efficiency of 23.2% was obtained. The low efficiency is primarily due to the P2P (direct evaluation) subroutine. With a large number of processes (i.e. $P \geq 64$) and a relatively small number of points (10 million), the communication overhead became non-negligible compared to the computational cost of evaluating interactions, despite the use of non-blocking MPI send and receive commands. This is a hardware-related problem rather than an algorithmic one. Better strong scaling efficiency could be expected if more points

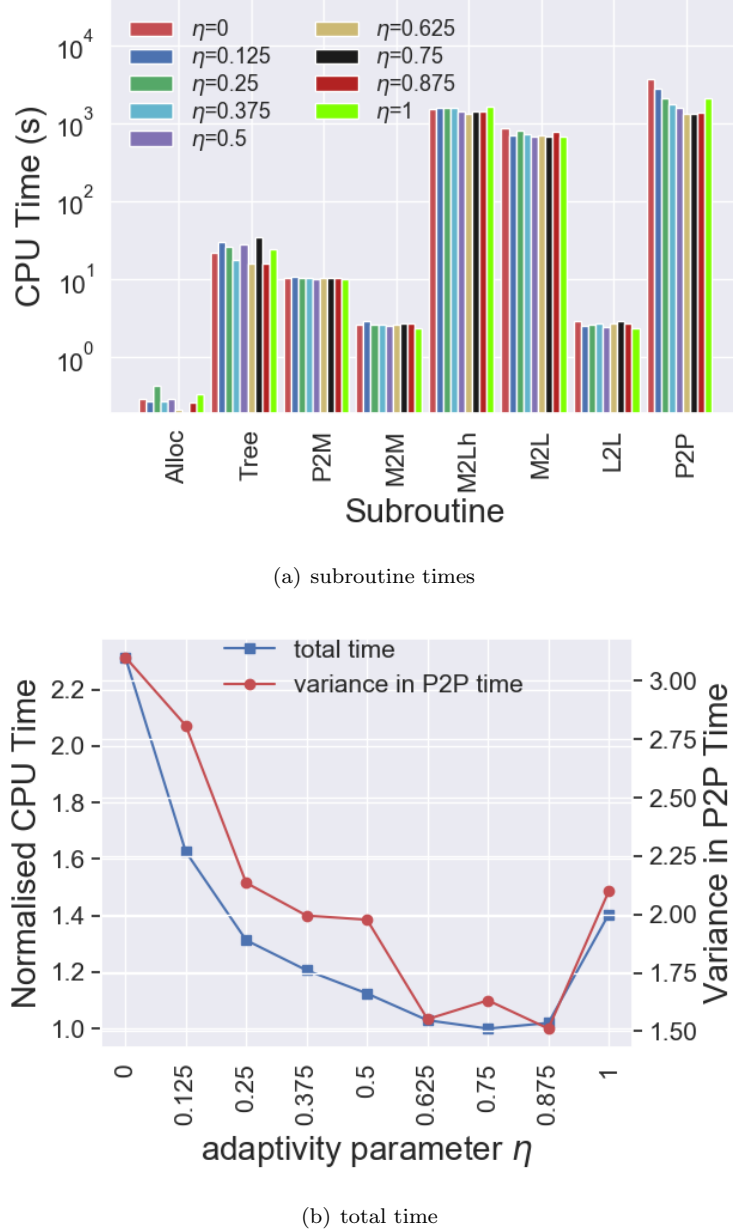


FIGURE 3.10. Sensitivity of galaxy simulation time to η . Simulation used 10^9 points, 512 processes and a 5 level tree.

were used because the latency would be hidden by higher computational cost. In this test, the number of points was limited by the single-core memory capacity.

Weak scaling efficiency of between 46% to 63% was obtained depending on the number of levels. Note that it is not possible to obtain 100% weak scaling efficiency

due to a geometric effect that results in increasing connectivity as the domain is divided into more subdomains. By accounting for this, we estimated an adjusted weak scaling efficiency of between 73% and 100% depending on the number of levels. Absolute computation times in the weak scaling tests were sensitive to the number of levels (i.e. to the number of points per leaf box) and displayed a convex response. With 1 million points per process the optimal values were 5 levels or equivalently 244 points per leaf box.

We investigated the effect of the adaptivity parameter η on performance. $\eta = 0$ corresponds to non-adaptive FMM (purely geometric box splitting), balancing the cost of the M2L shift. Conversely $\eta = 1$ corresponds to fully adaptive FMM (purely median splitting), balancing the cost of the P2P direct evaluation. Intermediate values, $0 < \eta < 1$, are thus a blend of both. The time taken to simulate gravitational attraction in a large-scale non-homogeneous point distribution had a convex response to η , meaning that it can be readily optimised. The optimal value $\eta = 0.75$ reduced computation time by a factor of more than 2 relative to the non-adaptive case ($\eta = 0$) and by a factor of 1.4 relative to the purely adaptive case ($\eta = 1$). The speedup is mainly attributed to reduced variation in the number of points per leaf box resulting in better load balancing and lower latency in the P2P direct interaction. Again we note that the convexity means that automatic optimisation could be beneficial, as was demonstrated previously in 2D [13].

Scaling performance of the Tree subroutine (halo matrix construction) was poor although it made a negligible contribution to total time in the range of P tested. The poor scaling was the result of receiving data in process number order, causing significant latency at large P . The dominant M2L and P2P subroutines used a more sophisticated approach whereby data was processed in the order in which the non-blocking receive commands were completed. P2P exhibited poor scaling when the number of levels was large owing to having a large number of leaf boxes. This caused the cluster's network to be flooded with a lot of small messages. Previous work [18] testing the code on the Lomonosov-2 machine suggested that the scalability limits are system-specific. More software engineering measures could be taken to improve the code performance.

For best performance in the most important context of time-dependent problems, continuous autotuning of parameters can be expected to be highly advantageous, as indicated by the earlier experiences in 2D [13]. An implementation issue is here to maintain and locally update the distributed FMM tree at a near optimal cost. This is also where the transparency of the implementation becomes a definite advantage.

ACKNOWLEDGMENT

This work was financially supported by the Swedish Research Council within the UPMARC Linnaeus center of Excellence (S. Engblom), by the Swedish strategic research programme eSENCE (J. Bull, S. Engblom), and partly supported by the The Swedish Foundation for international Cooperation in Research and Higher Education (STINT) Initiation Grant IB2016-6543, entitled 'Large scale complex numerical simulations on large scale complex computer facilities - identifying performance and scalability issues', 2016–2017. We are grateful to the Research Computing Center at the Moscow State University, Russia for granting us access to Lomonosov-2 where the galaxy simulations were performed. The scaling tests were performed on the Rackham cluster at UPPMAX provided by the Swedish National

Infrastructure for Computing (SNIC) and we are grateful for their support. We are also grateful to Masters students Anders Gärdenäs and David Ryman of Uppsala University for their work on testing early versions of the `daFMM3D` code.

REFERENCES

- [1] T. Askham and A. Cerfon. An adaptive fast multipole accelerated poisson solver for complex geometries. *Journal of Computational Physics*, 344:1 – 22, 2017. [doi:10.1016/j.jcp.2017.04.063](https://doi.org/10.1016/j.jcp.2017.04.063).
- [2] L. Barba and R. Yokota. How will the fast multipole method fare in the exascale era? *SIAM News*, 46(6), 2013.
- [3] R. Beatson and L. Greengard. *A short course on fast multipole methods*, pages 1–37. Oxford University Press, 1997.
- [4] H. Cheng, L. Greengard, and V. Rokhlin. A fast adaptive multipole algorithm in three dimensions. *J. Comput. Phys.*, 155(2):468–498, 1999. [doi:10.1006/jcp.1999.6355](https://doi.org/10.1006/jcp.1999.6355).
- [5] B. A. Cipra. The best of the 20th century: Editors name top 10 algorithms. *SIAM News*, 33(4), 2000.
- [6] P. Coulier, H. Pouransari, and E. Darve. The inverse fast multipole method: using a fast approximate direct solver as a preconditioner for dense linear systems. *SIAM Journal on Scientific Computing*, 39(3):A761–A796, 2017. [doi:10.1137/15M1034477](https://doi.org/10.1137/15M1034477).
- [7] F. Cruz, M. G. Knepley, and L. Barba. Petfmm - a dynamically load-balancing parallel fast multipole library. *Int. J. Numer. Methods Engrg.*, 85:403–428, 2011. [doi:10.1002/nme.2972](https://doi.org/10.1002/nme.2972).
- [8] S. Engblom. On well-separated sets and fast multipole methods. *Applied Numerical Mathematics*, 61:1096–1102, 2011. [doi:10.1016/j.apnum.2011.06.011](https://doi.org/10.1016/j.apnum.2011.06.011).
- [9] A. Gholami, D. Malhotra, H. Sundar, and G. Biros. FFT, FMM or multigrid? A comparative study of state-of-the-art Poisson solvers in the unit cube, 2014. URL <https://arxiv.org/abs/1408.6497>.
- [10] A. Goude and S. Engblom. Adaptive fast multipole methods on the GPU. *Journal of Supercomputing*, 63:897–918, 2013. [doi:10.1007/s11227-012-0836-0](https://doi.org/10.1007/s11227-012-0836-0).
- [11] L. Greengard and V. Rokhlin. A fast algorithm for particle simulations. *Journal of Computational Physics*, 73:325–348, 1987. [doi:10.1016/0021-9991\(87\)90140-9](https://doi.org/10.1016/0021-9991(87)90140-9).
- [12] N. A. Gumerov and R. Duraiswami. Fast multipole methods on graphics processors. *J. Comput. Phys.*, 227(18):8290–8313, 2008. [doi:10.1016/j.jcp.2008.05.023](https://doi.org/10.1016/j.jcp.2008.05.023).
- [13] M. Holm, S. Engblom, A. Goude, and S. Holmgren. Dynamic autotuning of adaptive fast multipole methods on hybrid multicore CPU and GPU systems. *SIAM Journal on Scientific Computing*, 36(4):376–399, 2014. [doi:10.1137/130943595](https://doi.org/10.1137/130943595).
- [14] H. Ibeid, R. Yokota, J. Pestana, and D. Keyes. Fast multipole preconditioners for sparse matrices arising from elliptic equations. *Computing and Visualization in Science*, 18(6):213–229, Mar 2018. [doi:10.1007/s0079](https://doi.org/10.1007/s0079).
- [15] Z. Jinshi, L. Yongmei, and J. S. Parallel FMM algorithm based on space decomposition. In *Ninth International Conference on Grid and Cloud Computing*, pages 168–173. IEEE, 2010. [doi:10.1109/GCC.2010.43](https://doi.org/10.1109/GCC.2010.43).

- [16] I. Lashuk, A. Chandramowlishwaran, H. Langston, T.-A. Nguyen, R. Sampath, A. Shringarpure, R. Vuduc, L. Ying, D. Zorin, and G. Biros. A massively parallel adaptive fast multipole method on heterogeneous architectures. *Commun. ACM*, 55:101–109, 2012. [doi:10.1145/1654059.1654118](https://doi.org/10.1145/1654059.1654118).
- [17] MathWorks, The. Spiral galaxy formation simulation using MATLAB function blocks, 2017. URL <http://www.mathworks.com/help/simulink/examples/spiral-galaxy-formation-simulation-using-matlab-function-blocks.html>. The MathWorks, Natick, MA, USA.
- [18] M. Neytcheva, S. Holmgren, J. Bull, A. Dorostkar, A. Kruchinina, D. Nikitenko, N. Popova, P. Shvets, A. Teplov, V. Voevodin, and V. Voevodin. Multidimensional performance and scalability analysis for diverse applications based on system monitoring data. In *Parallel Processing and Applied Mathematics*, Lecture Notes in Computational Science. Springer, 2017. [doi:10.1007/978-3-319-78024-5_37](https://doi.org/10.1007/978-3-319-78024-5_37).
- [19] B. Shanker and H. Huang. Accelerated Cartesian expansions - a fast method for computing of potentials of the form $R^{-\nu}$ for all real ν . *J. Comput. Phys.*, 226(1):732–753, 2007. [doi:10.1016/j.jcp.2007.04.033](https://doi.org/10.1016/j.jcp.2007.04.033).
- [20] J. Singh, C. Holt, J. Hennessy, and A. Gupta. A parallel adaptive fast multipole method. In *Supercomputing '93: Proceedings of the 1993 ACM/IEEE Conference on Supercomputing*. IEEE, 1993. [doi:10.1109/SUPERC.1993.1263424](https://doi.org/10.1109/SUPERC.1993.1263424).
- [21] H. Sundar, R. S. Sampath, and G. Biros. Bottom-up construction and 2:1 balance refinement of linear octrees in parallel. *SIAM J. Sci. Comput.*, 30(5):2675–2708, 2008. [doi:10.1137/070681727](https://doi.org/10.1137/070681727).
- [22] A. Toomre and J. Toomre. Galactic bridges and tails. *The Astrophysical Journal*, 178:623–666, 1972. [doi:10.1086/151823](https://doi.org/10.1086/151823).
- [23] M. Vikram, A. Baczewski, B. Shanker, and S. Aluru. Parallel accelerated Cartesian expansions for particle dynamics simulations. In *Proceedings of the 2009 IEEE International Parallel and Distributed Processing Symposium*, pages 1–11, 2009. [doi:10.1109/IPDPS.2009.5161038](https://doi.org/10.1109/IPDPS.2009.5161038).
- [24] M. Warren and J. Salmon. Astrophysical n-body simulations using hierarchical tree data structures. In *Supercomputing '92: Proceedings of the 1992 ACM/IEEE Conference on Supercomputing*. IEEE, 1992. [doi:https://doi.org/10.1109/SUPERC.1992.236647](https://doi.org/10.1109/SUPERC.1992.236647).
- [25] L. Ying, G. Biros, and D. Zorin. A kernel-independent adaptive fast multipole algorithm in two and three dimensions. *Journal of Computational Physics*, 196:591–626, 2004. [doi:10.1016/j.jcp.2003.11.021](https://doi.org/10.1016/j.jcp.2003.11.021).
- [26] R. Yokota. An FMM based on dual tree traversal for many-core architectures. *J. Algorithms and Comput. Tech.*, 7:301–324, 2013. [doi:10.1260/1748-3018.7.3.301](https://doi.org/10.1260/1748-3018.7.3.301).
- [27] R. Yokota and L. Barba. Treecode and fast multipole method for N-body simulation with CUDA. In W.-M. Hwu, editor, *GPU Computing Gems Emerald Edition*, chapter 9, pages 113–132. Morgan Kaufmann/Elsevier, 2011. [doi:10.1016/B978-0-12-384988-5.00009-7](https://doi.org/10.1016/B978-0-12-384988-5.00009-7).
- [28] R. Yokota, L. Barba, T. Narumi, and K. Yasuoka. Petascale turbulence simulation using a highly parallel fast multipole method on GPUs. *Computer Physics Communications*, 184:445–455, 2013. [doi:10.1016/j.cpc.2012.09.011](https://doi.org/10.1016/j.cpc.2012.09.011).
- [29] R. Yokota, G. Turkiyyah, and D. Keyes. Communication complexity of the fast multipole method and its algebraic variants, 2014. URL <https://arxiv.org>.

[org/abs/1406.1974](https://arxiv.org/abs/1406.1974).

[30] R. Yokota, H. Ibeid, and D. Keyes. Fast multipole method as a matrix-free hierarchical low-rank approximation, 2016. URL <https://arxiv.org/abs/1602.02244v1>.

APPENDIX A. ALGORITHMS

Algorithms for the construction of the tree, connectivity matrix and halo matrix, the downward pass of the balanced FMM tree, and the direct evaluation are presented here.

DIVISION OF SCIENTIFIC COMPUTING, DEPARTMENT OF INFORMATION TECHNOLOGY, UPPSALA UNIVERSITY, SE-751 05 UPPSALA, SWEDEN.

URL: <http://user.it.uu.se/~stefane>
E-mail address: stefane@it.uu.se

Algorithm 2 Tree, halo and connectivity matrix construction on process p .

Root level ($l=0$):

1: Construct root box $T_p^{(1)}$ and connectivity matrix $C_p^{(1)}$
2: **for** $q = 0 : P - 1, q \neq p$ **do**
3: Non-blocking send centre coords and radius of root box $T_p^{(1)}$ to q
4: Blocking receive centre coords and radius of root box $T_q^{(1)}$ from q
5: **if** $\text{theta_crit}(T_p^{(1)}, T_q^{(1)})$ **then**
6: $T_p^{(1)}, T_q^{(1)}$ weakly connected
7: **else**
8: $T_p^{(1)}, T_q^{(1)}$ strongly connected
9: **end if**
10: **end for**
11: *Loop over remaining levels:*
12: **for** $l=1:L$ **do**
13: Adaptive split of parents in $T_p^{(l-1)}$ into 8 children in $T_p^{(l)}$ according to η value
14: **for** $q = 0 : P - 1, q \neq p$ **do**
15: Compute no. of connections: $\text{ncon} = 64 \times$ strong connections in $H_{pq}^{(l-1)}$
16: Allocate space for lists of ncon connections: $H_{pq}^{(l)}.ibox, jbox$
17: Make $ilist, jlist$: children of strongly connected parents on p, q resp.
18: Non-blocking send centre coords and radii of $ilist$ to q
19: Non-blocking receive centre coords and radii of $jlist$ from q
20: **end for**
21: Construct local connectivity matrix $C_p^{(l)}$ on level l
22: **for** $q = 0 : P - 1, q \neq p$ **do**
23: Wait for receive from q to complete
24: Initialise indices: $fwd=0, bwd=ncon$
25: **for** $i \in ilist$ **do**
26: **for** $j \in jlist$ **do**
27: **if** $\text{theta_crit}(i, j)$ **then**
28: $T_{p,i}^{(l)}, T_{q,j}^{(l)}$ weakly connected
29: Set $H_{pq}^{(l)}.ibox[bwd]=i, H_{pq}^{(l)}.jbox[bwd]=j$
30: **bwd=bwd-1**
31: **else**
32: $T_{p,i}^{(l)}, T_{q,j}^{(l)}$ strongly connected
33: Set $H_{pq}^{(l)}.ibox[fwd]=i, H_{pq}^{(l)}.jbox[fwd]=j$
34: **fwd=fwd+1**
35: **end if**
36: **end for**
37: **end for**
38: **end for**

Algorithm 3 Downward pass of balanced FMM on process p .

Parallel M2L:

- 1: **for** $l = 1 : L - 1$ **do**
- 2: **for** $q = 0 : P - 1, q \neq p$ **do**
- 3: From $H_{pq}^{(l)}$ get boxes in p weakly connected to boxes in q
- 4: Start non-blocking send of box centre coords and coeffs from p to q
- 5: Start non-blocking receive box centre coords and coeffs from q to p
- 6: **end for**
- 7: Set $W = \{q : q \in [0 : P - 1] \mid q \text{ contains boxes weakly connected to } p\}$
- 8: **while** W is not empty **do**
- 9: **for** $q \in W$ **do**
- 10: **if** non-blocking receive from q has completed **then**
- 11: Asymmetric M2L shift from boxes in q to boxes in p
- 12: Remove q from set: $W = W - q$
- 13: **end if**
- 14: **end for**
- 15: **end while**
- 16: **end for**

M2L:

- 17: **for** $l = 2 : L - 1$ **do**
- 18: Symmetric M2L shift between boxes in p
- 19: **end for**

L2L:

- 20: **for** $l = 1 : L - 1$ **do**
- 21: L2L shift from boxes in p to their children
- 22: **end for**

Algorithm 4 Evaluation stage of balanced FMM on level L on process p .

Parallel P2P setup:

- 1: **for** $q = 0 : P - 1, q \neq p$ **do**
- 2: Get list of boxes in p strongly connected to boxes in q
- 3: Get point coordinates and masses in owned boxes
- 4: Start non-blocking send of box indices, coordinates and masses to q
- 5: Start non-blocking receive of box indices, coordinates and masses from q
- 6: **end for**

L2P (far-field contribution):

- 7: Evaluate local expansion at points in leaf boxes in p

P2P (near-field contribution):

- 8: Symmetric direct interactions between points in leaf boxes in p

Parallel P2P evaluation:

- 9: Set $S = \{q : q \in [0 : P - 1] \mid q \text{ contains boxes strongly connected to } p\}$
- 10: **while** S is not empty **do**
- 11: **for** $q \in S$ **do**
- 12: **if** non-blocking receive from q has completed **then**
- 13: Asymmetric direct interaction with points in leaf boxes in q
- 14: Remove q from set: $S = S - q$
- 15: **end if**
- 16: **end for**
- 17: **end while**
